NUMERICAL AND EXPERIMENTAL DETERMINATION OF SECONDARY SEPARATION AT THE LEEWARD SIDE OF A DELTA WING IN COMPRESSIBLE FLOW

ICAS-88-5.4.3

E.M. Houtman, W.J. Bannink
Delft University of Technology
Delft, The Netherlands

SUMMARY

The turbulent boundary layer flow at the leeward side of a planar delta wing at high angles of attack and high subsonic Mach numbers has been studied. A quasi-three dimensional boundary layer method has been developed, assuming a conical external flow and similar velocity profiles along rays through the apex. The solution takes place at a constant chord position, while the marching direction is away from an attachment line until separation is reached. The present method has been tested with experimental pressure distributions as input. The predicted surface flow compared with oil flow visualization tests showed good agreement as far as the limiting streamlines and the secondary separation positions are concerned.

NOTATION

C_{f_r}, C_{f_θ}	skin-friction coefficients
c_p	surface pressure coefficient
C_r	rootchord of the wing
E	ratio of total enthalpy
F,G	velocity ratios
H	total enthalpy
M	Mach number
Pr	Prandtl number
Pr_t	'turbulent' Prandtl number
p	pressure
q	$=(u^2 + v^2)^{1/2}$
Re_r	Reynolds number
r,θ,z	cylindrical coordinates
T	temperature
U	free stream velocity
u,v,w	velocity components in r,θ,z directions respectively
x,y,z'	cartesian coordinates
α	angle of attack
γ	ratio of specific heats
δ	boundary layer thickness
$\varepsilon_m, \varepsilon_{m_i}, \varepsilon_{m_o}$	eddy viscosity coefficients
ε_H	eddy conductivity coefficient
η	transformed z-coordinate
μ	dynamic viscosity coefficient, kg/ms
ν	kinematic viscosity coefficient, m^2/s
ρ	density
σ	$= \rho\mu u$
τ	shear stress
τ_t	turbulent shear stress
Φ, Ψ	stream functions
φ	angle of velocity vector on surface z=constant

Subscripts

e	edge of boundary layer
t	tangential
w	wall
∞	free stream conditions

INTRODUCTION

In the last years the interest in the flow around delta wings at high angles of attack has been increased considerably. This is mainly due to the development of fast manoevrable aircraft and missiles and to the growing capability of computing complex vortex-dominating flows[1]. Although the geometry of a delta wing is rather simple, it is rather difficult to obtain realistic computational results, especially for high angles of attack and high speed free stream conditions. The flow around a delta wing may be characterized by a strong viscid-inviscid interaction. The rolling-up of free shear-layers emanating from the leading edge has a major effect on the entire flow field, and consequently on the aerodynamic coefficients of the wing. With inviscid computational methods vortices emanating from sharp leading edges may be captured. This is not the case with free shear-layers shed off from a smooth surface. These are a result of boundary layer separation due to an adverse pressure gradient, so their position is not known a priory. The status of the boundary layer is very important. A turbulent boundary layer upstream of separation will sustain an adverse pressure gradient over a longer distance than a laminar boundary layer.

The computation of the boundary layer on a conical body like a delta wing upstream of separation will be discussed in this paper. The present method may be seen as a modification and extension of the methods developed by Matsuno[2], DeJarnette[3] and Adams[4]. The computational method is a simplified 3D- method, using the assumption of conical inviscid external flow. The conical flow concept is valid for supersonic flows; for high subsonic flows trailing edge effects will disturb it. From experiments however, it can be seen that certain phenomena like lines of attachment and separation occur along straight lines through the apex[1,5]. Furthermore pressure gradients in spanwise direction are much larger than chordwise pressure gradients, so the assumption of conical flow is rather good .

The present boundary layer method can be used in interaction with conical inviscid computational methods. If vortices emanating from a smooth surface can be modelled, the position of separation has to be prescribed. In order to improve the inviscid calculations, it would be necessary to predict the position of these separations by studying the evolution of the boundary layer upstream of separation.

In this paper only experimental pressure distributions have been used to generate boundary values. The experimental data were obtained from measurements in the transonic - supersonic windtunnel of the Delft University of Technology, Faculty of Aerospace Engineering[5]. The delta wing model had a sweep angle of 65° and a flat upper surface. It was tested at Mach numbers between 0.6 and 0.9 and at angles of attack of 5° - 22°. The calculations were made for $M_\infty = 0.6$, 0.7 and 0.85 and $\alpha = 5°$, 10° and 15°.

GOVERNING EQUATIONS

The turbulent boundary layer equations for a steady compressible flow will be described in an orthogonal curvi-linear (r,θ,z) coordinate system[6], fit to a conical body (fig. 1). In this system z is the normal distance to the surface, r is the distance to the apex and θ is the angle between a generator and a fixed generator measured along the unwrapped surface. The velocities u,v and w are in the directions r, θ and z respectively. Then the system of equations may be written as:

continuity

$$\frac{\partial}{\partial r}(r\rho u) + \frac{\partial}{\partial \theta}(\rho v) + \frac{\partial}{\partial z}(r\overline{\rho w}) = 0 \tag{1}$$

r-momentum

$$\rho u \frac{\partial u}{\partial r} + \frac{\rho v}{r}\frac{\partial u}{\partial \theta} + \overline{\rho w}\frac{\partial u}{\partial z} - \frac{\rho v^2}{r} = \rho_e u_e \frac{\partial u_e}{\partial r} + \frac{\rho_e v_e}{r}\frac{\partial u_e}{\partial \theta} - \frac{\rho_e v_e^2}{r} + \frac{\partial}{\partial z}\left(\mu \frac{\partial u}{\partial z} - \rho\overline{u'w'}\right) \tag{2}$$

θ-momentum

$$\rho u \frac{\partial v}{\partial r} + \frac{\rho v}{r}\frac{\partial v}{\partial \theta} + \overline{\rho w}\frac{\partial v}{\partial z} + \frac{\rho u v}{r} = \rho_e u_e \frac{\partial v_e}{\partial r} + \frac{\rho_e v_e}{r}\frac{\partial v_e}{\partial \theta} + \frac{\rho_e u_e v_e}{r} + \frac{\partial}{\partial z}\left(\mu \frac{\partial v}{\partial z} - \rho\overline{v'w'}\right) \tag{3}$$

energy

$$\rho u \frac{\partial H}{\partial r} + \frac{\rho v}{r}\frac{\partial H}{\partial \theta} + \overline{\rho w}\frac{\partial H}{\partial z} = \frac{\partial}{\partial z}\left(\frac{\mu}{Pr}\frac{\partial H}{\partial z} + \mu\left(1 - \frac{1}{Pr}\right)\frac{\partial}{\partial z}\left(\frac{u^2+v^2}{2}\right) - \rho\overline{w'H'}\right) \tag{4}$$

where H is the total enthalpy defined by

$$H = \frac{\gamma}{\gamma-1}\frac{p}{\rho} + \frac{u^2+v^2+w^2}{2} \tag{5}$$

The dynamic viscosity μ will be determined according to Sutherlands' law, and the Prandtl number is taken constant, Pr=0.7. The boundary conditions for (1)-(4) with an adiabatic wall are:

$$z=0:\ u,v,w=0;\ \frac{\partial H}{\partial z} = 0 \tag{6a}$$

$$z=\delta:\ u = u_e(r,\theta);\ v = v_e(r,\theta);\ H = H_e(r,\theta) \tag{6b}$$

where δ is the boundary layer thickness and the subscripts w,e denote quantities taken at the wall (z=0) and at the boundary layer edge, respectively. For the modeling of the turbulent Reynolds stresses the Cebeci-Smith eddy viscosity concept is used[7]:

$$-\rho\overline{u'w'} = \rho\varepsilon_m \frac{\partial u}{\partial z};\quad -\rho\overline{v'w'} = \rho\varepsilon_m \frac{\partial v}{\partial z} \tag{7a}$$

$$-\rho\overline{w'H'} = \rho\varepsilon_H \frac{\partial H}{\partial z} = \rho \frac{\varepsilon_m}{Pr_t}\frac{\partial H}{\partial z} \tag{7b}$$

ε_m is the eddy-viscosity coefficient, ε_H the eddy-conductivity coefficient and Pr_t is the 'turbulent' Prandtl number, $Pr_t = \frac{\varepsilon_m}{\varepsilon_H}$. ε_m is defined in an inner region near the surface by

$$\varepsilon_{m_i} = \left[0.4\, z\left(1-\exp\left(-\frac{z}{A}\right)\right)\right]^2 \left(\left(\frac{\partial u}{\partial z}\right)^2 + \left(\frac{\partial v}{\partial z}\right)^2\right)^{1/2} \tag{8}$$

where

$$A = 26\frac{\nu}{u_\tau}\left(\frac{\rho}{\rho_w}\right)^{1/2};\quad u_\tau = \left(\frac{\tau_{t_w}}{\rho_w}\right)^{1/2}$$

$$\tau_{t_w} = \mu_w\left(\left(\frac{\partial u}{\partial z}\right)_w^2 + \left(\frac{\partial v}{\partial z}\right)_w^2\right)^{1/2}$$

In the outer region ε_m is defined by

$$\varepsilon_{m_o} = 0.0168\left|\int_o^\infty (u_{t_e} - u_t)\, dz\right| \tag{9}$$

where $u_t = (u^2+v^2)^{1/2}$

The inner and outer region are established by the continuity of the eddy viscosity formula.

In order to reduce the number of dependent variables two streamfunctions are introduced, such that:

$$r\rho u = \frac{\partial \Psi}{\partial z},\quad \rho v = \frac{\partial \Phi}{\partial z} \tag{10}$$

Satisfying the continuity equation, Eq. (1), we obtain

$$r\overline{\rho w} = -\frac{\partial \Psi}{\partial r} - \frac{\partial \Phi}{\partial \theta} \tag{11}$$

We also transform the z coordinate into a nondimensional quantity by

$$\eta = \left(\frac{u_e}{\rho_e \mu_e r}\right)^{1/2}\int_o^z \rho\, dz \tag{12}$$

Then, two nondimensional functions may be derived satisfying

$$f(r,\theta,\eta(z)) = (\rho_e\mu_e u_e r)^{-1/2}\frac{1}{r}\Psi(r,\theta,z) \tag{13}$$

$$g(r,\theta,\eta(z)) = \frac{u_e}{V_e}(\rho_e\mu_e u_e r)^{-1/2}\Phi(r,\theta,z) \tag{14}$$

Using Eqs. (10)-(14) we may derive

$$u = u_e\frac{\partial f}{\partial \eta} = u_e F \tag{15a}$$

$$v = v_e\frac{\partial g}{\partial \eta} = v_e G \tag{15b}$$

Eqs. (7) and (10)-(14) may now be substituted into the boundary layer equations (2)-(4). Then it will be clear that the laminar boundary layer equations allow similar solutions along rays θ = constant if the external flow is conical, which means that the flow quantities are independent of r. The similarity transformation is equivalent to the Blasius transformation for a flat plate. This concept is not valid for turbulent boundary layers, since the eddy-viscosity terms are dependent on r. Several authors[4,8] have introduced the idea of local similarity, which means that the eddy-viscosity terms are locally independent on r while they are evaluated at the actual r position. This is a valid assumption if the flow quantities in the boundary layer vary sufficiently slow with r. Under the above mentioned local similarity restriction a transformation of the boundary layer equations into a parabolic system may be acomplished. The coordinate r only serves as a parameter; the coordinate θ is the time-like marching direction. Thus for a conical inviscid external flow the equations become:

$$\frac{\partial}{\partial\eta}\left(b\frac{\partial F}{\partial\eta}\right) + \left(Q + \frac{v_e}{u_e}\frac{\partial g}{\partial\theta}\right)\frac{\partial F}{\partial\eta} - \frac{v_e}{u_e}G\frac{\partial F}{\partial\theta} = R_1 \qquad (16)$$

$$\frac{\partial}{\partial\eta}\left(b\frac{\partial G}{\partial\eta}\right) + \left(Q + \frac{v_e}{u_e}\frac{\partial g}{\partial\theta}\right)\frac{\partial G}{\partial\eta} - \frac{v_e}{u_e}G\frac{\partial G}{\partial\theta} = R_2 \qquad (17)$$

$$\frac{1}{Pr}\frac{\partial}{\partial\eta}\left(b\frac{\partial E}{\partial\eta}\right) + \left(Q + \frac{v_e}{u_e}\frac{\partial g}{\partial\theta}\right)\frac{\partial E}{\partial\eta} - \frac{v_e}{u_e}G\frac{\partial E}{\partial\theta} = -\frac{\partial R_3}{\partial\eta} \qquad (18)$$

where

$$Q = \frac{3}{2}f + \left(\frac{v_e}{2u_e\sigma_e}\frac{d\sigma_e}{d\theta} + \frac{d}{d\theta}\left(\frac{v_e}{u_e}\right)\right)g$$

$$\sigma_e = \rho_e\mu_e u_e$$

$$E = H/H_e$$

$$b = \frac{\rho\mu}{\rho_e\mu_e}\left(1 + \frac{\rho\varepsilon_m}{\mu}\right)$$

$$R_1 = \left(\frac{v_e}{u_e}\right)^2\left(FG - G^2\right)$$

$$R_2 = FG + \frac{1}{u_e}\frac{dv_e}{d\theta}G^2 - \frac{\rho_e}{\rho}\left(1 + \frac{1}{u_e}\frac{dv_e}{d\theta}\right)$$

$$R_3 = \frac{u_e^2\left(1 - \frac{1}{Pr}\right)\rho\mu}{\rho_e\mu_e H_e}\left(F\frac{\partial F}{\partial\eta} + \frac{v_e^2}{u_e^2}G\frac{\partial G}{\partial\eta}\right)$$

The boundary conditions are:

$$\eta=0:\ f=F=0;\ g=G=0;\ \frac{\partial E}{\partial\eta} = 0 \qquad (19a)$$

$$\eta=\eta_e:\ F=G=E=1 \qquad (19b)$$

Eqs. (16)-(18) are solved starting at an attachmentline, where $v=v_e=0$ and $\frac{dv_e}{d\theta} > 0$. The solution is marched in θ-direction until separation is reached. In the case of conical flow this means that the skinfriction coefficient in θ-direction becomes zero.

The skinfriction coefficients in r and direction are defined by:

$$c_{f_r} = \frac{2\left(\mu\frac{\partial u}{\partial z}\right)_w}{\rho_\infty U_\infty^2} = \frac{2}{(Re_r)^{1/2}}\left(\frac{u_e}{U_\infty}\right)^2\left(\frac{\sigma_\infty}{\sigma_e}\right)^{1/2}\left(\frac{\rho}{\rho_\infty}\frac{\mu}{\mu_\infty}\frac{\partial F}{\partial\eta}\right)_w \qquad (20)$$

$$c_{f_\theta} = \frac{2\left(\mu\frac{\partial v}{\partial z}\right)_w}{\rho_\infty U_\infty^2} = \frac{2}{(Re_r)^{1/2}}\frac{u_e v_e}{U_\infty^2}\left(\frac{\sigma_\infty}{\sigma_e}\right)^{1/2}\left(\frac{\rho}{\rho_\infty}\frac{\mu}{\mu_\infty}\frac{\partial G}{\partial\eta}\right)_w \qquad (21)$$

However, on the reattacment line $G=v/v_\theta$ is indeterminate and the limit on this line has to be taken at this position. It may be shown that G is finite at the reattachment line and that the starting solutions may be obtained from Eqs. (16)-(18). They reduce to the ordinary differential equations

$$\frac{d}{d\eta}\left(b\frac{dF}{d\eta}\right) + Q\frac{dF}{d\eta} = 0 \qquad (22)$$

$$\frac{d}{d\eta}\left(b\frac{dG}{d\eta}\right) + Q\frac{dG}{d\eta} = FG + \frac{1}{u_e}\frac{dv_e}{d\theta}\left(G^2 - \frac{\rho_e}{\rho}\right) - \frac{\rho_e}{\rho} \qquad (23)$$

$$\frac{1}{Pr}\frac{d}{d\eta}\left(b\frac{dE}{d\eta}\right) + Q\frac{dE}{d\eta} = \frac{u_e^2\left(1-\frac{1}{Pr}\right)}{H_e}F\frac{dF}{d\eta}\frac{\rho\mu}{\rho_e\mu_e} \qquad (24)$$

DETERMINATION OF THE INVISCID VELOCITY

For the boundary layer calculations we need the velocity components u_e and v_e as boundary conditions. Normally they are obtained from an inviscid flow code. In the case of an experimental data they have to be derived from a measured pressure distribution.

On the body of the surface (z=0,w=0) the conical inviscid equations may be written as:

$$\frac{du}{d\theta} - v = 0 \qquad (25)$$

$$v\frac{dv}{d\theta} + uv + \frac{1}{\rho}\frac{dp}{d\theta} = 0 \qquad (26)$$

$$\frac{\gamma}{\gamma-1}\left(\frac{p}{\rho} - \frac{p_\infty}{\rho_\infty}\right) + \frac{1}{2}\left(u^2+v^2-U_\infty^2\right) = 0 \qquad (27)$$

If we transform the velocity components into

$$u = q\cos\varphi,\quad v = q\sin\varphi \qquad (28)$$

where q is the speed of the inviscid surface flow and the angle of the velocity vector with a conical ray, we obtain from Eqs. (25) and (26) for isentropic flow

$$\frac{q^2}{U_\infty^2} = 1 + \frac{2}{\gamma-1}\frac{1}{M_\infty^2}\left(1 - \left(\frac{p}{p_\infty}\right)^{\frac{\gamma-1}{\gamma}}\right) \qquad (29)$$

and

$$\left(1 + \frac{d\varphi}{d\theta}\right)\tan\varphi + \frac{\frac{1}{p_\infty}\frac{dp}{d\theta}}{\gamma\left(\frac{p}{p_\infty}\right)^{1/\gamma}\left[M_\infty^2 + \frac{2}{\gamma-1}\left(1 - \left(\frac{p}{p_\infty}\right)^{\frac{\gamma-1}{\gamma}}\right)\right]} = 0 \qquad (30)$$

Eq. (30) can be solved numerically for a given spanwise pressure distribution and given starting values of φ and $\frac{d\varphi}{d\theta}$. On a reattachment line this equation is indeterminate. This problem may be dealt with by differentiation of Eq. (30). The result on the reattachment line is

$$\frac{d\varphi}{d\theta} = -\frac{1}{2} + \frac{1}{2}\left[1 - \frac{\frac{4}{p_\infty}\frac{d^2p}{d\theta^2}}{\gamma\left(\frac{p}{p_\infty}\right)^{1/\gamma}\left[M_\infty^2 + \frac{2}{\gamma-1}\left(1 - \left(\frac{p}{p_\infty}\right)^{\frac{\gamma-1}{\gamma}}\right)\right]}\right]^{1/2} \tag{31}$$

FINITE DIFFERENCE METHOD

The transformed boundary layer equations (16)-(18) are to be solved using a marching procedure. These equations are of a parabolic nature, so an implicit difference scheme is preferred to avoid instability problems. If a fully implicit scheme is used, the non-linear terms have to be linearized with a Newton method; this implies an iteration procedure. In the present method an alternative is applied by using a predictor-corrector linearization following Matsuno[2] and DeJarnette and Woodson[3]. This so called 'half-implicit' scheme is implicit in the η-(z-) direction and explicit in the θ-direction. Thus the scheme is second order accurate, unconditionally stable and no iteration procedure is needed.

For the determination of the initial profiles at an reattachment line, Eqs. (22)-(24) are discretized using the same η-differences. Using a Newton linearization for the nonlinear terms the differential equations are solved in an iteration procedure.

The following notations are used in the finite difference equations:

$$U_{i,j} = U(\theta_i, \eta_j) \tag{32}$$

where

$$\theta_{i+1} = \theta_i + \Delta\theta_i \quad ; \; i = 1,2,.....IMAX-1 \tag{33a}$$

$$\eta_{j+1} = \eta_j + \Delta\eta_j \quad ; \; j = 1,2,.....JMAX-1 \tag{33b}$$

The central difference operators are defined by

$$\Delta_\eta U_{i,j} = \frac{U_{i,j+1} - U_{i,j-1}}{\Delta\eta_j + \Delta\eta_{j-1}} \tag{34}$$

$$\delta_\eta U_{i,j+\frac{1}{2}} = \frac{U_{i,j+1} - U_{i,j}}{\Delta\eta_j} \tag{35}$$

$$\delta_\theta U_{i+\frac{1}{2},j} = \frac{U_{i+1,j} - U_{i,j}}{\Delta\theta_i} \tag{36}$$

$$\delta_\eta\left(b_{i,j}\delta_\eta U_{i,j}\right) = \frac{2}{\Delta\eta_j+\Delta\eta_{j-1}}\left(b_{i,j+\frac{1}{2}}\frac{U_{i,j+1}-U_{i,j}}{\Delta\eta_j} - b_{i,j-\frac{1}{2}}\frac{U_{i,j}-U_{i,j-1}}{\Delta\eta_{j-1}}\right) \tag{37}$$

with $b_{i,j\pm\frac{1}{2}} = \frac{1}{2}\left(b_{i,j} + b_{i,j\pm1}\right)$.

For the predictor step the backward difference operator

$$\nabla_\theta U_{i+\frac{1}{2},j} = \frac{U_{i+\frac{1}{2},j} - U_{i,j}}{\frac{1}{2}\Delta\theta_i} \tag{38}$$

is used.
The discretization of $\frac{\partial f}{\partial \eta} = F$ becomes

$$\delta_\eta f_{i,j+\frac{1}{2}} = \frac{f_{i,j+1} - f_{i,j}}{\Delta\eta_j} = \frac{1}{2}\left(F_{i,j+1} - F_{i,j}\right)$$

from which we may write

$$f_{i,j+1} = f_{i,j} + \frac{1}{2}\Delta\eta_j\left(F_{i,j} + F_{i,j+1}\right) \tag{39}$$

A similar expression holds for g.

The predictor stage becomes

$$\delta_\eta\left(b_{i,j}\delta_\eta F_{i+\frac{1}{2},j}\right) + \left(Q_{i,j} + \left(\frac{v_e}{u_e}\right)_{i+\frac{1}{2}}\nabla_\theta g_{i+\frac{1}{2},j}\right)\Delta_\eta F_{i,j} - \left(\frac{v_e}{u_e}\right)_{i+\frac{1}{2}} G_{i,j}\nabla_\theta F_{i+\frac{1}{2},j} = \left(R_1\right)_{i,j} \tag{40}$$

and similar expressions for G and E. The relation between f,g and F,G, respectively, is obtained from Eq. (39).

For the corrector-stage the equations are

$$\delta_\eta\left(b_{i+\frac{1}{2},j}\delta_\eta\left(\frac{F_{i,j}+F_{i+1,j}}{2}\right)\right) + \left(Q_{i+\frac{1}{2},j} + \left(\frac{v_e}{u_e}\right)_{i+\frac{1}{2}}\delta_\theta g_{i+\frac{1}{2},j}\right)\Delta_\eta F_{i+\frac{1}{2},j} - \left(\frac{v_e}{u_e}\right)_{i+\frac{1}{2}} G_{i+\frac{1}{2},j}\,\delta_\theta F_{i+\frac{1}{2},j} = \left(R_1\right)_{i+\frac{1}{2},j} \tag{41}$$

and similar expressions for G and E.
The difference equations may be written in a block-tridiagonal matrix form. The system of equations is solved using a modified Davis algorithm[9]. The solution marches away from an attachment line in cross-flow direction until the skin friction coefficient c_{f_θ} becomes less than zero. This means that separation occurs, and the solution of the boundary layer equations breaks down.
For the turbulent calculations a variable grid was employed[9]:

$$\eta_j = \frac{\eta_{JMAX}\left(K^{(j-1)\Delta N/\Delta N_o} - 1\right)}{K^{1/\Delta N_o} - 1} \tag{42}$$

where η_{JMAX} is an appropriate choice after some iterations of the determination of the initial profiles; $\Delta N = 1/JMAX$; $\Delta N0 = 0.1$; $K = 1.5$. The mesh width $\Delta\theta$ was varied such that it decreased in regions of large $\frac{dv_e}{d\theta}$

DISCUSSION OF RESULTS

Experiments

The experimental results[5] were obtained from measurements on a delta wing with a flat upper surface, sharp leading edges and a sweep angle of 65°. The results used for the calculations cover free stream Mach numbers of 0.6, 0.7 and 0.85 and angles of attack of 5°, 10° and 15°.
The experiments contain oilflow visualizations of the surface flow and measurements of the surface pressure distribution. The pressure tabs are located at a spanwise row at 70% root chord, at a row at the rootchord and at some different spanwise stations. The latter were applied to check the amount of conicity of the flow and the existence of non-conical shock waves at high angles of attack and high Mach numbers. The Reynolds number based on the rootchord varied from 3 to 3.6×10^6.

A sketch of the vortex flow at the leeward side of a delta wing is given in fig. 2. The primary vortices emanate from the sharp leading edges as a result of the merging of the boundary layers from upper- and lower side. The flow reattaches at the lines A1. These lines move towards the rootchord as the angle of attack increases, and will coincide at the wing symmetry line (rootchord) above a certain angle of attack.

Due to the primary vortices the pressure from the attachmentline towards the leading edge first decreases, reaches a suction peak and then increases considerably. This unfavourable pressure gradient will cause the flow to separate, which will lead to the formation of a secondary vortex. This separation is of the so called 'open-type' separation, which is a much more stable phenomenon than the closed bubble separation in two-dimensional flow. The existence of a secondary vortex will have a large influence on the pressure distribution, and thus on the aerodynamic characteristics of the wing.

The experiments in the high-subsonic flow regime showed that the pressure distribution is not conical. At the rootchord an almost linear pressure increase was measured. The pressure gradients in spanwise direction, especially in the suction peak region are much larger than the pressure gradients in chordwise direction. Thus a conical approximation will be a good first approach, as will be shown when comparing the computational and the experimental results.

All calculations are carried out for a turbulent boundary layer. This assumption is valid for the chord position where the pressure distribution is measured. From the oil flow visualization pictures an outboard shift of the secondary separation line could be observed at x/Cr = 0.2-0.25 . This has certainly to do with the transition from a laminar to a turbulent boundary layer.

It should be noted that if the outer flow may no longer be regarded as conical, which may be due to embedded shock waves, trailing edge- or tip effects, vortex bursting, the present method can not be used. Also the non-conical transition region can not be covered by the method.

Computations

As shows Table 1, the theoretical and experimental results compare rather well for almost all cases studied. Therefore only one case for the highest Mach number (0.85) and a moderate angle of attack (10°) has been included in this paper. In fig. 3 the pressure distribution for this case is shown, together with the distribution of the velocity components u_e and v_e derived from the pressure distribution with (29)-(31). This result serves as an input to the boundary layer calculations. The calculations were carried out with 80 gridpoints in η-direction and with spanwise steps of $\Delta\theta = 0.004$ rad = 0.23 deg.

The resulting distributions of the skinfriction coefficients in spanwise (c_{f_θ}) and radial (c_{f_r}) direction are shown in fig. 4. The deviations in c_{f_θ} are much larger than the deviation in c_{f_r}. The position of secondary separation is indicated by the point where c_{f_θ} crosses zero ($0.6 < y/yle < 0.8$). The radial component C_{f_r}, however, does not become zero at this position. This theoretically obtained secondary separation position is slightly inboard of the experimentally observed line in the oil flow pattern (see fig.5). In the following table some different cases are summarized, showing that the overall result seems to be rather good.

M	α (°)	S_2 % of local semi-span		diff.
		exp.	theor.	
0.6	5	82.2	81.3	0.9
0.6	10	77.4	76.1	1.3
0.6	15	73.9	72.9	1.0
0.7	10	75.8	74.6	1.2
0.7	15	72.8	68.6	4.2
0.85	5	80.6	80.9	-0.7
0.85	10	73.2	70.5	3.2

Table 1. Location of secondary (turbulent) separation .

It should be noted that the calculations break down just behind separation. This has to do with the Goldstein singularity, appearing in direct calculations near separation.

An possible reason for the differences between experimental and computational separation positions could be the lack of a good resolution in the experimental pressure distribution. The pressure orifices located in the region of interest are located with intervals of 6% semi-span. This involves that the position of minimum c_p in the splined c_p-distribtion can differ to the order of some percents to the real position. This has a large influence on the computations.

At higher angles of attack and higher Mach numbers the assumption of conical flow becomes less valid due to the influence of vortex bursting, shock-waves etc. This will cause increasing discrepancies between theoretical and experimental results. These aspects have not been studied here.

For comparison with the oil flow visualization the limiting streamlines may be derived from the skin friction coefficients. The limiting streamline angle φ_w and the outer streamline angle φ_e are shown in fig. 5. Also the measured values φ_w from the oilflow pictures have been plotted; it shows a rather good agreement with the theoretical results, especially in the region of increasing . Beyond the suction peak an inflection point in the φ_w-distribution through the boundary layer appears, so the decrease in φ_w is much larger than in φ_e.

The calculated streamline pattern is given in fig. 6. This may be compared with the picture of the oilflow pattern in fig. 7.

The spanwise and chordwise momentum thicknesses are plotted in fig. 8. Just inboard of the location of minimum pressure the momentum thickness reaches a minimum; before separation it increases considerably.

CONCLUDING REMARKS

A quasi-three dimensional boundary layer method for compressible turbulent flows has been developed. Oil flow visualization tests have shown that the surface flow on planar delta wings may be considered as nearly conical over a large part of the wing. This is due to the observation that in the region of interest for the boundary layer computations the gradients of pressure are much larger in the spanwise than in the chordwise direction. This phenomenon validates the assumption of a conical outer flow, which simplifies the originally three dimensional problem to a great extent.

The present boundary layer method was tested on experimental pressure distributions. It has been shown that the method provides a good possibility to compute the surface flow and to predict separation lines. This was verified with oil flow visualization data. Furthermore the non-iterative difference scheme is rather cheap in terms of computer time.

Further investigation is needed for the coupling with a method for the inviscid outer flow field. For the incompressible case some attempts have been made. From the work of de Bruin and Hoeijmakers[10] it is known that the coupling of a direct boundary layer method with a panel method in which the secondary vortex is modeled, does not lead to a useful prediction of the position of secondary separation. In order to overcome this a complex strong interaction procedure, as indicated by Riley[11], is necessary. A different approach is followed by Wai e.a.[12], who used a scheme with a radial (chordwise) marching direction, the entire secondary vortex can be captured within the boundary layer. Since no back flow in radial direction occurs, no difficulties are encountered. The coupling with the method for the outer flow (without modeling the secondary vortex) is provided by the displacement thickness. The results seem to be rather good.

REFERENCES

1. Elsenaar, A. and Eriksson, G., Eds., Proceedings of the Symposium on International Vortex Flow Experiment on Euler Code Verification, Oct. 1986 Stockholm, FFA, Sweden.
2. Matsuno, K., A Vector-oriented Finite Difference Scheme for Calculating Three-Dimensional Compressible Laminar and Turbulent Boundary Layers on Practical Wing configurations, AIAA-81-1020, 1981.
3. DeJarnette, F.R. and Woodson, S.H., Numerical and Experimental Determination of Secondary Separation on Delta Wings in Subsonic Flow, AIAA J. of Aircraft, Vol. 22, No. 7, pp.602-608, 1985.
4. Adams, Jr, J.C., Finite-Difference Analysis of the Three-Dimensional Turbulent Boundary Layer on a Sharp Cone at Angle of Attack in a Supersonic Flow, AIAA 72-186, 1972.
5. Ottochian, S.P., Bannink, W.J. and Houtman, E.M., Investigation of the Vortex Flow over a Sharp-Edged Delta Wing in the Transonic Speed Regime, Delft University of Technology, To be published, 1988.
6. Cebeci, T., Kaups, K. and Ramsey, J. A General Method for Calculating Three Dimensional Compressible Laminar and Turbulent Boundary Layers on Arbitrary Wings, NASA CR-2777, 1977.
7. Cebeci, T. and Smith, A.M.O., Analysis of Turbulent Boundary Layers, Academic Press, New York, 1974.

8. Bontoux, P. and Roux, B., Compressible Turbulent Boundary Layer on a Yawed Cone, AIAA 75-858, 1975.
9. Blottner, F.G., Introduction to Computational Techniques for Boundary Layers, Sandia Laboratories, Albuquerque, Rep. 79-0893, 1979.
10. De Bruin, A.C. and Hoeijmakers, H.W.M. Computation of Three-Dimensional Boundary Layer Transition and Separation on a 65 deg. Swept Delta Wing at 20 deg. Angle of Attack, NLR MP 86075U, Amsterdam, 1986, also in Ref. 1.
11. Riley, N., Separation from a Smooth Surface in a Slender Conical Flow, J. of Eng. Mathmetics, Vol.13, no.1, pp.75-91, 1979.
12. Wai, J.C., Baillie, J.C. and Yoshihara, H., Computation of Turbulent Separated Flows over Wings, in: Numerical and Physical Aspects of Aerodynamic Flows III, ed. T. Cebeci, 1985, Springer Verlag, New York.

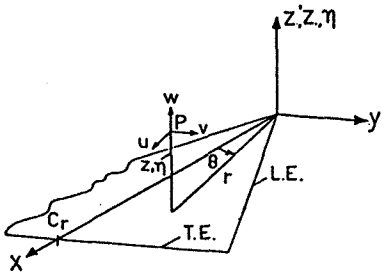

Fig. 1. Coordinate system

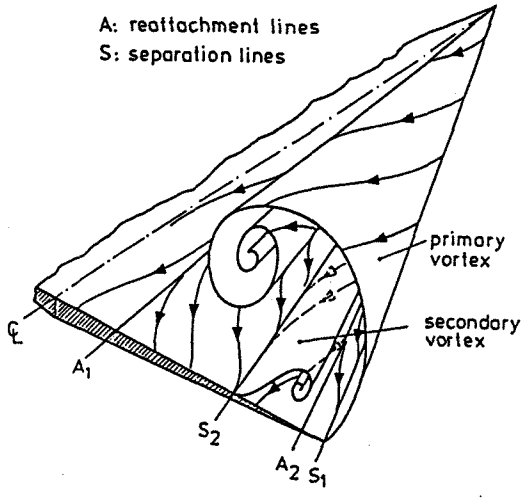

Fig. 2. Delta wing leeward flow geometry

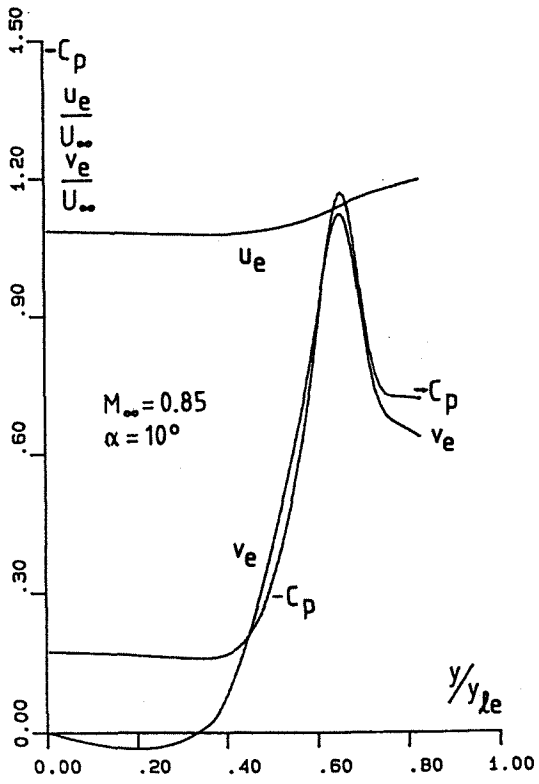

Fig. 3. Experimental pressure coefficient and inviscid velocity components.

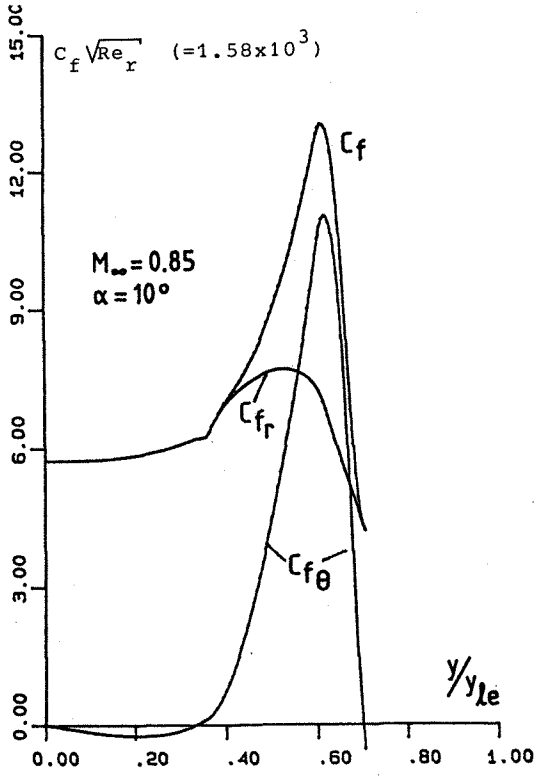

Fig. 4. Skin friction coefficients.

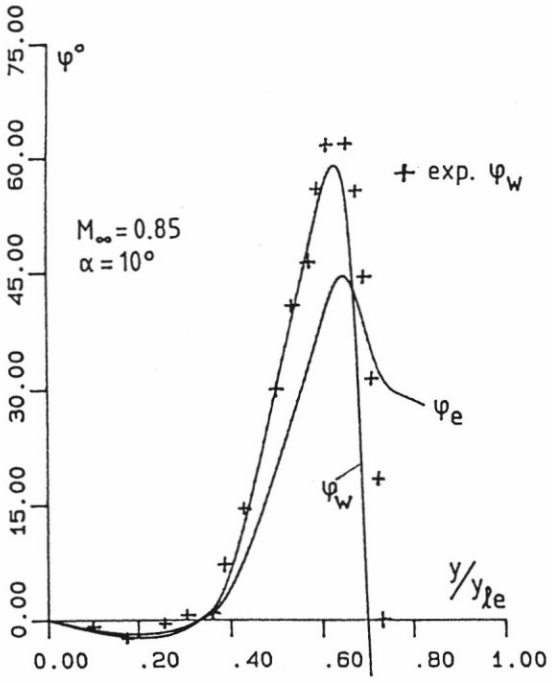

Fig. 5 . Surface flow directions

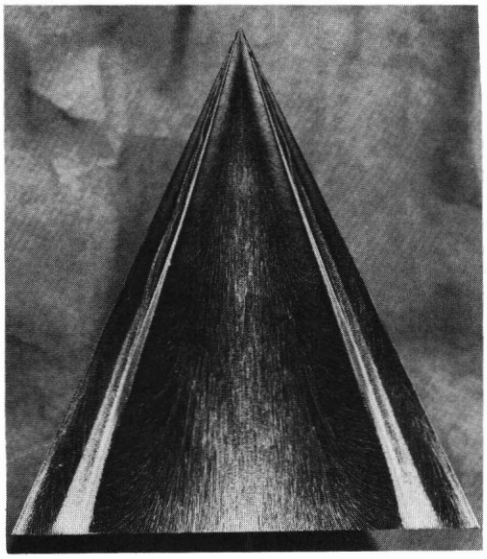

Fig. 7. Oil flow pattern ($M_\infty = 0.85$, $\alpha = 10^\circ$).

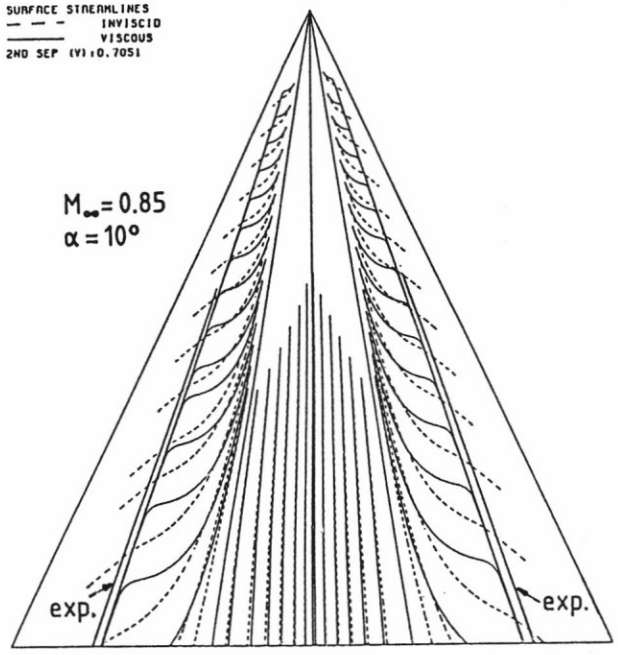

Fig. 6. Surface streamlines and separation lines.

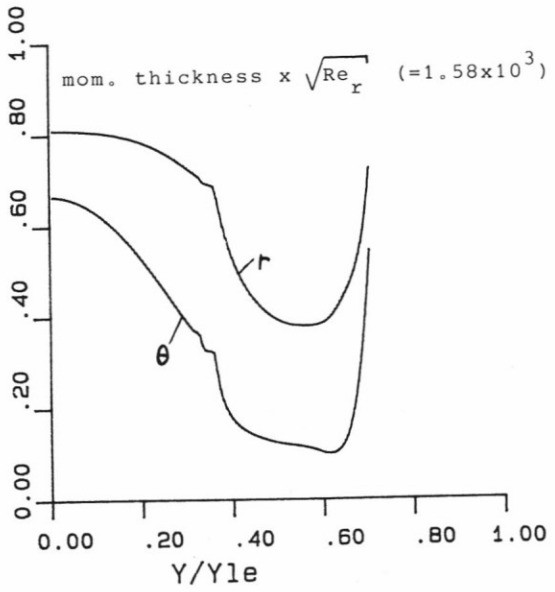

Fig. 8. Distribution of momentum thicknesses.